J. Plasma Physics (2010), *vol.* 76, *parts* 3&4, *pp.* 369–375.
doi:10.1017/S0022377809990559

Full-scale simulation study of stimulated electromagnetic emissions: The first ten milliseconds

BENGT ELIASSON[1]† and LENNART STENFLO[2]

[1]Theoretische Physik IV, Ruhr-Universität Bochum, DE-44780, Bochum, Germany (bengt@tp4.rub.de)

[2]Department of Physics, Linköping University, SE-581 83, Linköping, Sweden

(Received 18 November 2009 and accepted 1 December 2009, first published online 15 January 2010)

Abstract. A full-scale numerical study is performed of the nonlinear interaction between a large-amplitude electromagnetic wave and the Earth's ionosphere, and of the stimulated electromagnetic emission emerging from the turbulent layer, during the first 10 milliseconds after switch-on of the radio transmitter. The frequency spectra are downshifted in frequency and appear to emerge from a region somewhat below the cutoff of the O mode, which is characterized by Langmuir wave turbulence and localized Langmuir envelopes trapped in ion density cavities. The spectral features of escaping O-mode waves are very similar to those observed in experiments. The frequency components of Z-mode waves, trapped in the region between the O- and Z-mode cutoffs show strongly asymmetric and downshifted spectra.

1. Introduction

There is a continuing interest in the nonlinear interaction and turbulence in the ionosphere, induced by high-power radio transmitters. The plasma turbulence is usually studied by ground-based radars, while the escaping stimulated electromagnetic emission (SEE) is recorded by ground-based receivers. A number of nonlinear processes have been identified, including three-wave decay of the electromagnetic wave into Langmuir and ion acoustic waves (the so called parametric decay instability), Langmuir turbulence, and the formation of cavitons (Stenflo and Shukla 1997, 2000; Kuo 2001, 2003). The nonlinear interaction between intense radar beams with ion velocity gradients (Shukla and Stenflo 1992) and the Farley–Buneman modes in the Earth's atmosphere (Shukla et al. 2002) have also been considered. In a non-uniform weakly-ionized magnetoplasma in the lower part of the Earth's ionosphere, the nonlinear interaction of powerful radio waves with non-resonant density fluctuations may lead to the filamentation of radio waves (Shukla et al. 1992). These and many other phenomena are discussed in reviews of recent experimental and theoretical results (Stenflo 2004; Gurevich 2007). Numerical studies include simulations of parametric processes associated with

† Also at: Department of Physics, Umeå University, SE-901 87 Umeå, Sweden.

upshifted ionospheric stimulated radiation (Scales and Xi 2000) and nonlinear evolution of thermal self-focusing instabilities in inhomogeneous ionospheric plasmas (Gondarenko et al. 2006).

In this paper, we present the results of large-scale simulations using a generalized Zakharov model based on a recent work (Eliasson and Stenflo 2008), but using a more realistic model of the ion and electron Landau damping. Our previous studies (Eliasson and Stenflo 2008; Eliasson et al. 2008) have shown the parametric decay and the formation of cavitons, as well as the generation of topside turbulence by Z-mode waves generated at the turbulent layer close to the O-mode cutoff (Eliasson 2008). Here we are interested in the spectral features of the electromagnetic field at different altitudes, including the escaping radiation that propagates out from the plasma and the trapped Z-mode radiation above the O-mode cutoff.

2. Mathematical model

In our one-dimensional simulation geometry, we assume that a large-amplitude electromagnetic wave is injected vertically, along the z axis, into the vertically stratified ionospheric layer. The mathematical model, derived by Eliasson and Stenflo (2008), is based on a separation of timescales, where the time-dependent quantities (here denoted $\psi(z,t)$) are separated into a slow and a high-frequency time scale, $\psi = \psi_s + \psi_h$. The high-frequency component is assumed to take the form $\psi_h = (1/2)[\widetilde{\psi}(z,t)\exp(-i\omega_0 t) + \text{complex conjugate}]$, where $\widetilde{\psi}$ represents the slowly varying complex envelope of the high-frequency field, and ω_0 is the frequency of the transmitted electromagnetic wave. Hence the time derivatives on the fast timescale will be transformed as $\partial/\partial t \to \partial/\partial t - i\omega_0$ when going from the ψ_h variable to the $\widetilde{\psi}$ variable. The dynamics of the high-frequency electromagnetic waves and electron dynamics is coupled nonlinearly to the slow timescale electron dynamics via the ponderomotive force acting on the electrons, and is mediated to the ions via the electrostatic field on the slow timescale.

We first present the envelope equations of the high-frequency fields, in the presence of low-frequency plasma fluctuations. The transverse (to the z axis) components of the electromagnetic field in the presence of a slowly varying electron density n_{es} is governed by the electromagnetic wave equation

$$\frac{\partial \widetilde{\mathbf{A}}_\perp}{\partial t} = i\omega_0 \widetilde{\mathbf{A}}_\perp - \widetilde{\mathbf{E}}_\perp, \tag{2.1}$$

$$\frac{\partial \widetilde{\mathbf{E}}_\perp}{\partial t} = i\omega_0 \widetilde{\mathbf{E}}_\perp - c^2 \frac{\partial^2 \widetilde{\mathbf{A}}_\perp}{\partial z^2} + \frac{e n_{es} \widetilde{\mathbf{v}}_{e\perp}}{\varepsilon_0}, \tag{2.2}$$

where $\widetilde{\mathbf{A}}_\perp$ and $\widetilde{\mathbf{E}}_\perp$ is the transverse vector potential (in Coulomb gauge) and electric field, respectively. Here c is the speed of light in vacuum and ε_0 is the vacuum permittivity. The z component of the electric field is governed by the Maxwell equation

$$\frac{\partial \widetilde{E}_z}{\partial t} = i\omega_0 \widetilde{E}_z + \frac{e n_{es} \widetilde{v}_{ez}}{\varepsilon_0}. \tag{2.3}$$

The high-frequency electron dynamics is governed by the continuity and momentum equation

$$\frac{\partial \widetilde{n}_e}{\partial t} = i\omega_0 \widetilde{n}_e - \frac{\partial (n_{es} \widetilde{v}_{ez})}{\partial z}, \tag{2.4}$$

https://doi.org/10.1017/S0022377809990559 Published online by Cambridge University Press

and

$$\frac{\partial \widetilde{\mathbf{v}}_e}{\partial t} = i\omega_0 \widetilde{\mathbf{v}}_e - \frac{e}{m_e}(\widehat{\mathbf{z}}\widetilde{E}_z + \widetilde{\mathbf{E}}_\perp + \widetilde{\mathbf{v}}_e \times \mathbf{B}_0) - \widehat{\mathbf{z}}\frac{3v_{Te}^2}{n_0}\frac{\partial \widetilde{n}_e}{\partial z} - \nu_e \widetilde{\mathbf{v}}_e, \qquad (2.5)$$

respectively, where $\mathbf{B}_0$ is the geomagnetic field, ν_e is the electron collision frequency, e is the magnitude of the electron charge, m_e is the electron mass, $v_{Te} = (k_B T_e/m_e)^{1/2}$ is the electron thermal speed, k_B is Boltzmann's constant, T_e is the electron temperature, and n_0 is the background electron number density. We have assumed that the ions are stationary on the fast timescale due to their large mass.

Next, we turn to the dynamics of the slowly varying plasma fluctuations, driven by the ponderomotive force of the high-frequency field. The slowly varying electron number density is separated as $n_{es} = n_{e0}(z) + n_s(z,t)$, where $n_{e0}(z) = n_{i0}(z)$ represents the large-scale electron density profile due to ionization/recombination in the ionosphere, and n_s is the slowly varying electron density fluctuations. We regard the electrons as inertialess on the slow time scale, where also quasi-neutrality $n_{is} = n_{es} \equiv n_s$ has been assumed. The ions are assumed to be unmagnetized, since the frequency of the ion fluctuations (a few kHz) is much larger than the ion gyrofrequency (about 50 Hz). The dynamics of the ions is governed by the continuity equation

$$\frac{\partial n_s}{\partial t} + n_0 \frac{\partial v_{iz}}{\partial z} = 0, \qquad (2.6)$$

and, since the ions are assumed to be unmagnetized, the slow timescale plasma velocity is obtained from the ion momentum equation driven by the ponderomotive force

$$\frac{\partial v_{iz}}{\partial t} = -\frac{C_s^2}{n_0}\frac{\partial n_s}{\partial z} - 2\nu_i * v_{iz} - \frac{\varepsilon_0}{4m_i n_0}\frac{\partial |\widetilde{\mathbf{E}}|^2}{\partial z} \qquad (2.7)$$

where $C_s = [k_B(T_e + 3T_i)/m_i]^{1/2}$ is the ion acoustic speed, T_i is the ion temperature, m_i is the ion mass, and we have denoted $|\widetilde{\mathbf{E}}|^2 = |\widetilde{\mathbf{E}}_\perp|^2 + |\widetilde{E}_z|^2$ and $|\widetilde{\mathbf{E}}_\perp|^2 = |\widetilde{E}_x|^2 + |\widetilde{E}_y|^2$. The ion Landau damping operator is defined as

$$\nu_i * v_{iz} = -C_s \left(\frac{T_e}{T_i}\right)^{3/2} \exp\left(-\frac{T_e}{2T_i}\right) \frac{1}{\sqrt{8\pi}} \int_0^\infty \frac{v_{iz}(z+\xi) - 2v_{iz}(z) + v_{iz}(z-\xi)}{\xi^2}\, d\xi. \qquad (2.8)$$

In the linear limit, this gives the ion dispersion relation $\omega = -i\widehat{\nu}_i + \sqrt{-\widehat{\nu}_i^2 + C_s^2 k^2} \approx -i\widehat{\nu}_i + C_s k$ with $\widehat{\nu}_i(k) = C_s|k|(T_e/T_i)^{3/2}\exp(-T_e/2T_i)\sqrt{\pi/8}$ in agreement with kinetic theory.

The electron Landau damping is in Fourier space given by

$$\nu_e(k) = \nu_{en} + \left(\frac{\pi}{8}\right)^{1/2} \frac{\omega_{pe}}{|k\lambda_{De}|^3} \exp\left[-\frac{1}{2(k\lambda_{De})^2}\right], \qquad (2.9)$$

where ν_{en} is the electron–neutral collision frequency, $\lambda_{De} = V_{Te}/\omega_{pe}$ is the electron Debye radius, and $\omega_{pe} = (n_0 e^2/\varepsilon_0 m_e)^{1/2}$ is the electron plasma frequency. The electron Landau damping is important only when the wavelength is large enough so that $k\lambda_{De}$ is larger than ~ 0.25. We are primarily interested in smaller wavenumbers, and for numerical convenience we therefore use a simplified approximation of

https://doi.org/10.1017/S0022377809990559 Published online by Cambridge University Press

the electron Landau damping operator as $\nu_e(k) = \nu_{en} + 0.5\omega_{pe}(\lambda_{De}k)^2$, which damps out waves efficiently for $\lambda_{De}k > 0.25$. In real space, we have $\nu_e * v = \nu_{en}v - 0.5\omega_{pe}\lambda_{De}^2\partial^2 v/\partial z^2$.

3. Numerical setup

We next define the simulation setup and physical parameters used in the simulation; the details of the numerical implementation and the discretization of variables are described in the Appendix of Eliasson and Stenflo (2008). The simulation code uses a one-dimensional geometry, along the z axis. Our simulation box starts at an altitude of 200 km and ends at 300 km. Our simulation code is based on a non-uniform nested grid method (Eliasson 2007). While $\widetilde{\mathbf{A}}_\perp$ and $\widetilde{\mathbf{E}}_\perp$ are represented on a grid with grid size $\delta z = 2$ m everywhere, the rest of the quantities $\widetilde{n}_e$, $\widetilde{\mathbf{v}}_e$, n_s, v_{iz}, and $\widetilde{E}_z$ are resolved with a much denser grid of grid size $\delta z = 2$ cm at the bottomside interaction region, $z = 277.5$–278.5 km, in order to resolve small-scale structures and electrostatic turbulence. The bottomside interaction region is thus at the same altitude as in Eliasson and Stenflo (2008) (where L_1 and L_2 in Appendix A of Eliasson and Stenflo (2008) should be 277.5 km and 278.5 km, not the misprinted 77.5 km and 78.5 km). Outside these regions, all quantities are resolved on the 2-m grid. This nested grid procedure is used to avoid a severe Courant–Friedrich–Levy (CFL) condition $\delta t < \delta z/c$, which would appear if the electromagnetic field would be resolved on the dense grid δz (Eliasson 2007). The ionospheric density profile is assumed to have a Gaussian shape of the form $n_{i0}(z) = n_{0,max}\exp[-(z - z_{max})^2/L^2]$, where $n_{0,max} = 5 \times 10^{11}$ m^{-3} and $z_{max} = 300$ km are the maximum density and the altitude of the F peak, and $L = 31.6$ km is the density scale length. The external magnetic field B_0 is set to 4.8×10^{-5} T and is tilted $\theta = 0.2269$ rad (13°) to the vertical (z) axis so that $\mathbf{B}_0 = B_0[\widehat{\mathbf{x}}\sin(\theta) - \widehat{\mathbf{z}}\cos(\theta)]$, which is the case at EISCAT in Tromsø. We assume that the transmitter on ground has been switched on at $t = 0$. The simulation starts at $t = 0.67$ ms, when the electromagnetic wave has reached the altitude 200 km. Initially, all time-dependent fields are set to zero, and random density fluctuations of order 10^6 m^{-3} are added to n_s to seed the parametric instability in the plasma. The electromagnetic wave is injected from the bottomside of the simulation box at 200 km, by setting the x component of the electric field to 1 V/m on the upward propagating field (see Eliasson and Stenflo 2008). The transmitter frequency is set to $\omega_0 = 2\pi \times 5 \times 10^6$ s^{-1}. We use oxygen ions so that $m_i = 16\, m_p$ where $m_p = 1836\, m_e$ is the proton mass. Further, $T_e = 2000$ K and $T_i = 1000$ K so that $v_{Te} = 1.7 \times 10^5$ m s^{-1} and $C_s = 1.6 \times 10^3$ m s^{-1}, and we use $n_0 = 3.1 \times 10^{11}$ m^{-3}, which is the electron number density at the altitude where $\omega = \omega_{pe}$. For these parameters, the X, O, and Z modes have their cutoffs (turning points) at $z \approx 273$ km, $z \approx 278$ km, and $z \approx 285$ km, respectively (Eliasson and Stenflo 2008). The electron–neutral collision frequency is set to $\nu_{en} = 10^3$ s^{-1}. The ion Landau damping operator (2.8) is approximated numerically as

$$\nu_i * v_{iz} \approx -C_s\left(\frac{T_e}{T_i}\right)^{3/2}\exp\left(-\frac{T_e}{2T_i}\right)\frac{1}{\sqrt{8\pi}}\sum_{j=1}^{N}\alpha_j\frac{v_{iz,i+j} - 2v_{iz,i} + v_{iz,i-j}}{(j\delta z)^2}\,\delta z, \quad (3.1)$$

where we have chosen $N = 40$, and the coefficients $\alpha_1 = 1.5$, $\alpha_j = 1$, $j = 2, \ldots, N$. The second derivative appearing in the electron Landau damping operator is approximated with a centered difference scheme. A fourth-order Runge–Kutta

https://doi.org/10.1017/S0022377809990559 Published online by Cambridge University Press

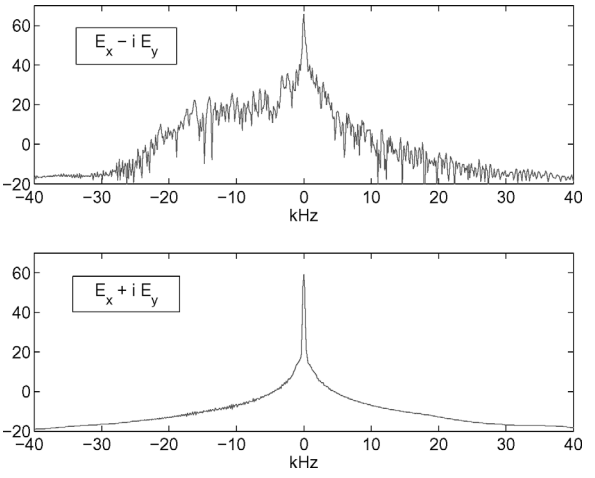

Figure 1. Power spectra (decibel) at $z = 200$ km, in the neutral atmosphere, for left-hand (top panel) and right-hand (bottom panel) polarized waves.

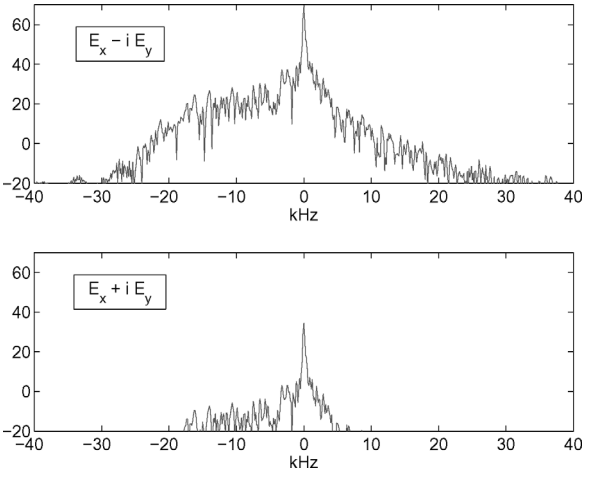

Figure 2. Power spectra (decibel) of O-mode waves at $z = 274$ km, between the the X- and O-mode cutoffs, for left-hand (top panel) and right-hand (bottom panel) polarized waves.

algorithm is used to advance the solution in time, with time step size $\delta t = 8 \times 10^{-9}$ s and 1.25×10^6 time steps.

4. Numerical results

The frequency spectra as functions of the frequency offset δf from the pump frequency $f_0 = \omega_0/2\pi$ are shown in Figs. 1–3 for different altitudes z. The spectra for left-hand polarization $E_x - iEy$ correspond roughly to O-mode polarization, while right-hand polarization $E_x + iEy$ corresponds to roughly X-mode spectra; we are interested in the main features and have neglected that the waves are in reality elliptically polarized due to the oblique geomagnetic field. In the determination of the polarization, it has been taken into account that the geomagnetic field is

https://doi.org/10.1017/S0022377809990559 Published online by Cambridge University Press

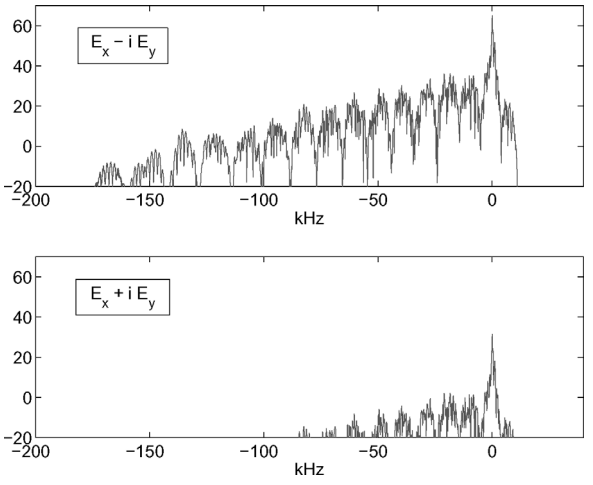

Figure 3. Power spectra (decibel) of Z-mode waves at $z = 282$ km, between the O- and Z-mode cutoffs, for left-hand (top panel) and right-hand (bottom panel) polarized waves.

pointed almost vertically with a negative z component. The whole simulation time series was used to construct the spectra, using a Hamming window. It is clearly seen in all figures that the wide SEE spectra are dominant for the left-hand O-mode polarization, while the X-mode spectra show no or only weak components different from the pump wave. In Fig. 1, which shows the frequency spectrum below the ionosphere at an altitude of 200 km, one can see that the O-mode spectrum is downshifted and extends about 20–30 kHz below the pump frequency. The up-shifted spectral components are considerably weaker. The spectra are very similar to the ponderomotive narrow continuum component in SEE spectra observed in experiment (Frolov et al. 2004). It is interesting to further investigate the source of the downshifted components. In Fig. 2, the frequency spectra at the altitude $z = 274$ km are displayed. This altitude is above the cutoff of the X mode, but below the cutoff of the O mode, and therefore the X mode is evanescent and only the O mode can contribute to the spectrum. The O-mode polarized spectrum in Fig. 2 shows almost identical features as in Fig. 1, which is another indication that the down-shifted spectra emerges from the turbulent layer below the O-mode cutoff. Finally, in Fig. 3, we show frequency spectra above the O-mode cutoff but below the Z-mode cutoff. Here the frequency spectrum is also concentrated to the left-hand polarized component, but is distinctly wider than the spectra in Figs. 1 and 2. It shows clear features of multiple inverse cascades towards lower frequencies.

5. Discussion

In summary, the frequency spectra of SEE have been studied by means of a full-scale numerical simulation of the nonlinear interaction between large-amplitude electromagnetic waves and the Earth's ionosphere. It is found that the electromagnetic O-mode first decays into ion-acoustic and two counter-propagating Langmuir waves, which in turn collapse into localized wave packets and ion density cavities in a region somewhat below the O-mode cutoff. The turbulent region radiates both O-mode waves, which propagate down out of the ionosphere, and Z-mode waves, which propagate upwards to their cutoff where they are reflected. The frequency spectra

https://doi.org/10.1017/S0022377809990559 Published online by Cambridge University Press

are asymmetric and downshifted, in agreement with experimental observations (Frolov et al. 2004). The trapped Z-mode waves exhibit a wide and downshifted frequency spectrum, indicating multiple inverse cascades towards lower frequencies. Future extensions may involve dusty plasma (Shukla and Mamun 2002) in the ionosphere, where parametric instabilities can be induced by large-amplitude electromagnetic waves (Shukla et al. 2004).

Acknowledgement

This work was supported by the Swedish Research Council (VR).

References

Eliasson, B. 2007 A nonuniform nested grid method for simulations of RF induced ionospheric turbulence. *Comput. Phys. Commun.* **178**, 8.

Eliasson, B. 2008 Full-scale simulation study of the generation of topside ionospheric turbulence using a generalized Zakharov model. *Geophys. Res. Lett.* **35**, L11104.

Eliasson, B. and Stenflo, L. 2008 Full-scale simulation study of the initial stage of ionospheric turbulence. *J. Geophys. Res.* **113**, A02305, doi:10.1029/2007JA012837.

Eliasson, B., Stenflo, L. and Shukla, P. K. 2008 Full-scale numerical modeling of turbulent processes in the Earth's ionosphere. *AIP Conf. Proc.* **1061**, 197.

Frolov, V. L., Sergeev, E. N., Komrakov, G. P., Stubbe, P., Thidé, B., Waldenvik, M., Veszelei, E., Leyser, T. B. 2004 Ponderomotive narrow continuum (NCp) component in stimulated electromagnetic emission spectra. *J. Geophys. Res.* **109**, A07304, doi: 10.1029/2001JA005063.

Gondarenko, N. A., Ossakow, S. L. and Milikh, G. M. 2006 Nonlinear evolution of thermal self-focusing instability in ionospheric modifications at high latitudes: aspect angle dependence. *Geophys. Res. Lett.* **33**, L16104, doi:10.1029/2006GL025916.

Gurevich, A. V. 2007 Nonlinear effects in the ionosphere. *Phys.-Usp.* **50**, 1091.

Kuo, S. P. 2001 Cascade of parametric instabilities in ionosphere heating experiments. *J. Plasma Phys.* **66**, 315.

Kuo, S. P. 2003 On parametric instabilities in HF heating of the ionosphere. *J. Plasma Phys.* **69**, 529.

Scales, W. A. and Xi, H. 2000 Theoretical and numerical simulation investigation of parametric processes associated with up-shifted ionospheric stimulated radiation. *Phys. Scripta* **T84**, 184.

Shukla, P. K. and Stenflo, L. 1992 Influence of a high-power radio wave on velocity gradient driven instabilities in the auroral F region ionosphere. *J. Geophys. Res.* **97**(A2), 1313.

Shukla, P. K., Stenflo, L. and Borisov, N. D. 1992 Nonlinear interaction of powerful radio waves with the plasma in the Earths lower ionosphere. *J. Geophys. Res.* **97**(A8), 12279.

Shukla, P. K. and Mamun, A. A. 2002 *Introduction to Dusty Plasma Physics*. Institute of Physics.

Shukla, P. K., Stenflo, L., Rosenberg, M. and Resendes, D. P. 2002 Dynamics of Farley-Buneman fluctuations in the presence of radar beams. *J. Geophys. Res.* **107**(A10), 1311, doi: 10.1029/2002JA009408.

Shukla, P. K., Eliasson, B. and Stenflo, L. 2004 Stimulated scattering of intense radio waves in partially ionized space dusty plasmas. *J. Geophys Res.* **109**, A03301.

Stenflo, L. and Shukla, P. K. 1997 Comments on the parametric excitation of low-frequency electrostatic waves. *J. Atm. Sol. Terr. Phys.* **59**, 2431.

Stenflo, L. and Shukla, P. K. 2000 Theory of stimulated scattering of large-amplitude waves. *J. Plasma Phys.* **64**, 353.

Stenflo, L. 2004 Comments on stimulated electromagnetic emissions in the ionospheric plasma. *Phys. Scripta* **T107**, 262.